Supporting Information for

Simultaneous Cationic and Anionic Ligand Exchange For Colloidally Stable $CsPbBr_3$ Nanocrystals

Muhammad Imran[†Δ], Palvasha Ijaz[†Δ], Luca Goldoni[⊥], Daniela Maggioni[‡], Urko Petralanda[†], Mirko Prato[Φ], Guilherme Almeida[†], Ivan Infante[§†*] and Liberato Manna[†*]

[†]Department of Nanochemistry, [⊥]Analytical Chemistry Facility and [Φ]Materials Characterization Facility, Istituto Italiano di Tecnologia, Via Morego 30, 16163 Genova, Italy

[Δ]Dipartimento di Chimica e Chimica Industriale, Università degli Studi di Genova, Via Dodecaneso 31, 16146 Genova, Italy

[‡] Dipartimento di Chimica, Università degli Studi di Milano, Via Golgi 19, 20133 Milano, Italy

[§] Department of Theoretical Chemistry, Faculty of Science, Vrije Universiteit Amsterdam, de Boelelaan 1083, 1081 HV Amsterdam, The Netherlands

Contents

Materials

Lead acetate trihydrate ($(PbAc_2 \cdot 3H_2O)$, 99.99%), caesium carbonate (Cs_2CO_3, reagent Plus, 99%), benzoyl bromide (C_6H_5COBr, 97%), acetone (99.5%), ethyl acetate (98.8%), toluene (anhydrous, 99.5%), didodecyldimethylammonium bromide (DDDMAB), didecyldimethylammonium bromide (DDMAB), dioctyldimethylammonium bromide (DODMAB), tetraoctylammonium bromide (TOAB), octadecene (ODE, technical grade, 90%), toluene-d8 (99 atom. % D), dodecyldimethyl ammine, hydrobromic acid (HBr, 48% aqueous solution) and oleic acid (OA, 90%), were purchased from Sigma-Aldrich. Didodecylamine (DDDAm, 97%), was purchased from TCI. All chemicals were used without any further purification.

Preparation of secondary and tertiary ammonium bromides

Didodecylammonium bromide and dodecyldimethyl ammonium bromide were prepared by reacting HBr with the corresponding amines in ethanol at 0ºC. Briefly, 50 mL of ethanol and 19 mmol of didodecylamine or dodecyldimethyl amine were mixed in a 100 mL 2-neck flask and vigorously stirred. This mixture was cooled in an ice-water bath, then 4.28 mL of HBr were added to it and the resulting mixture was allowed to react for 10 hours under N_2 flow. Then the solution was dried under vacuum and the solid product was purified by rinsing it with diethylether at least 6 times. Finally the white precipitate was dried overnight in vacuum oven at 80ºC and stored in glove box for further use.

Synthesis of $CsPbBr_3$ nanocubes

Oleate capped $CsPbBr_3$ NCs are synthesized following our previously reported procedure using standard Schlenk line techniques.[1] Briefly, lead (II) acetate trihydrate (76 mg) caesium carbonate (16 mg) and octadecene (10 ml) were combined in a 25 ml 3-neck flask equipped with a thermocouple and a magnetic stirrer. The reaction mixture was degassed for 5 minutes at room temperature and then for one hour at 115 °C. Then, a ligand mixture containing oleic acid (1.5 mL, previously degassed for an hour at 120 °C and stored in glove box), didodecylamine (1.25 mmol, 443 mg) dissolved in 1 mL of anhydrous toluene was rapidly injected under nitrogen. After the complete dissolution of the metal precursors, the temperature was decreased to 70 °C and a solution of benzoyl bromide (50 µL) in octadecene (500 µL, previously degassed for an hour at 120 °C and stored in glove box) was swiftly injected. After 60 seconds, the reaction mixture was cooled down by using a water bath and was directly used for ligand exchange reactions.

Ligand Exchange and Washing

All ligands exchange reactions were performed under air. Briefly, the crude reaction mixture containing the $CsPbBr_3$ NCs (3 mL) was treated with an anhydrous toluene solution containing the ammonium bromide salt (2 mL, 0.025M) and the mixture was vigorously stirred for 1 minute. Thereafter, the NCs were washed by addition of 15 mL of ethyl acetate followed by centrifugation at 6000 rpm for 10 minutes and re-dispersion in toluene. Additional cycles of ligand exchange were carried out by re-dispersing the NCs in a toluene solution containing the quaternary ammonium bromide salt (1 mL, 2 mM) and washing the NC dispersion with 6 mL of ethyl acetate. This procedure could be repeated several times (at least up to 3 times) without compromising the integrity of the final NCs. We note that excess of DDDMAB leads to degradation of the NCs. The control Cs-oleate capped sample was washed in a similar way, the only difference being that pure toluene was used instead (i.e. without any ammonium bromide).

Methods

X-ray Diffraction (XRD). The samples were prepared by drop casting concentrated NC dispersions onto a zero-diffraction silicon substrate and the diffraction patterns were acquired on a PANanalytical Empyrean X-ray diffractometer equipped with a 1.8 kW Cu K_α ceramic X-ray detector, operating at 45 kV and 40 mA using parallel beam geometry and symmetric reflection mode.

Transmission Electron Microscopy (TEM). Bright field TEM images were acquired on samples prepared by drop-casting diluted colloidal solutions on carbon film-coated 200 mesh copper grids, using a JEOL-1100 microscope operating at an acceleration voltage of 100 kV.

Steady-state UV-VIS Absorbance and Photoluminescence. Absorbance and photoluminescence spectra of dilute toluene dispersions in quartz cuvettes (1-cm path length) were recorded using a Varian Cary 300 UV-VIS spectrophotometer. The photoluminescence spectra were acquired using an excitation wavelength of 350 nm.

Photoluminescence Quantum Yields and Time-Correlated Single-Photon Counting. The time-resolved photoluminescence spectra and the absolute quantum yields were measured using an Edinburgh Instruments FLS920 spectrofluorometer. The PL decay traces were recorded by exciting the samples at 405 nm using a 50 ps laser diode. The data were collected at the PL peak position with an emission bandwidth of 10 nm. The photoluminescence quantum efficiencies were measured using the same instrument with an integrating sphere, exciting the nanocrystal solution at 400 nm (radiation from Xenon lamp). The optical density of the NC dispersions was 0.12±0.03 at 400 nm.

X-ray Photoelectron Spectroscopy (XPS). Measurements were performed on a Kratos Axis Ultra DLD spectrometer, using a monochromatic Al K_α source (15kV, 20mA). The photoelectrons were detected at a take-off angle of $\phi = 0°$ with respect to the surface normal. The pressure in the analysis chamber was kept below 7×10^{-9} Torr for data acquisition. The data was converted to VAMAS format and processed using CasaXPS software, version 2.3.17. The binding energy (BE) scale was internally referenced to the C 1s peak (BE for C-C = 284.8 eV).

Computational Modelling. The simulations were performed in vacuum at the DFT level of theory using the CP2K code[2] and employing the PBE exchange-correlation functional[3] and a double ζ basis set plus polarization functions[4]. Scalar relativistic effects have been accounted for by using effective core potential functions in the basis set. Spin-orbit coupling effects were not included in the calculations. For ground state relaxations, a default force convergence threshold of 4.5×10^{-4} Ha/bohr was used. For the computation of steric effects we used a passivation of 9 ligands on a facet in adjacent Cs sites, *i.e* each surface Cs cation is substituted by a DDDMAB cation, similar to the previous reports[5]. For the calculation of the electronic properties we extend the passivation to all facets, keeping the same ligand density per facet, but using shorter alkyl chains on the ammonium cations (tetramethyl ammonium cations substituting Cs^+) in order to facilitate calculations.

Nuclear magnetic resonance.

We used a Bruker Avance III 400 MHz spectrometer, equipped with a Broad Band Inverse probe (BBI) for the *quantitative* NMR spectra (*q*-NMR), ^{1}H NMR spectra at variable temperature, 2D ^{1}H-^{1}H NOESY (Nuclear overhauser effect spectroscopy) and 2D ^{1}H-^{13}C HSQC (*multiplicity edited* Heteronuclear Single Quantum Coherence) experiments.

All NMR chemical shifts were referred to the TMS (tetramethylsilane) internal reference signal, contained in toluene-d_8 solvent, calibrated at 0.0 ppm both for ^{1}H and for ^{13}C, while we referred all the ^{1}H chemical shifts in DMSO-d_6 solution, to the not deuterated residual solvent peak at 2.50 ppm.

The ^{1}H *q*-NMR spectrum for the analyses of composition in ligands was acquired in DMSO-d_6, at 300 K, after an automatic 90° pulse optimization. 32 transients were accumulated, with 64 k data points, without steady scans and with a relaxation delay of 30 s, over a spectral width of 20.55 ppm (offset at 6.18 ppm), at a fixed but optimized receiver gain, set at 64.

The ^{1}H NMR spectrum for ligand (DDDMAB) characterization was performed in toluene-d_8 by using identical parameters but 8 transients and a receiver gain set at 9.

The ^{1}H NMR spectra at different temperatures (300-353 K) were acquired in toluene-d_8, with tube spinning. The temperature was actively monitored and the samples remained in the probe for at least 2 min after the target temperature was reached, prior to acquisition. Afterwards, 8 transients were accumulated with a relaxation delay of 30 s, at a fixed receiver gain (45.2), over a spectral width of 20.02 ppm (offset at 6.175 ppm).

An exponential apodization equivalent of 0.3 Hz was applied to FIDs before Fourier Transform.

2D ^{1}H-^{1}H NOESY (noesygpph of the Bruker library) experiments were performed on toluene-d_8 dispersions of NCs and on toluene-d_8 solutions of DDDMAB, both at 300K and at 232K. A mixing time of 300 ms and a relaxation delay of 2.5 s were used with 2048 data points for direct and 256 for the indirect dimensions, by accumulating 8 transients.

2D ^{1}H-^{13}C HSQC (*multiplicity edited* Heteronuclear Single Quantum Coherence, hsqcedetgp, of the Bruker library) spectrum for DDDMAB characterization was acquired in toluene-d_8, using 2 transients, 1024 data points and 256 increments, with an automatic spectral width and transmitter frequency offset optimization for ^{1}H and a spectral width of 165 ppm (offset at 75 ppm) for ^{13}C.

We used a Bruker Avance III 600 MHz spectrometer equipped with a 5-mm QCI cryoprobe with z shielded pulsed-field gradient coil for the DDDMAB NCs characterization in toluene-d_8.

2D ^{1}H-^{13}C HSQC (*multiplicity edited* Heteronuclear Single Quantum Coherence, hsqcedetgp, of the Bruker library) spectrum for the DDDMAB NCs characterization was acquired in toluene-d_8, using 48 transients, 2018 data points and 256 increments, with an automatic spectral width and transmitter frequency offset optimization for ^{1}H and a spectral width of 165.6 ppm (offset at 74.6 ppm) for ^{13}C.

2D Diffusion Ordered Spectroscopy (DOSY). DOSY experiments were acquired on a Bruker DRX400 spectrometer (400.13 MHz) equipped with a Bruker 5 mm BBI Z-gradient probe headaffording a maximum gradient strength of 53.5 G/cm at 297 K, and using a ledbp pulse sequence with a diffusion time (Δ) of 100 ms and a total gradient pulse duration (δ) of 4 ms for NC or 1.2 ms for free ligand. The gradient

strength (G) was linearly incremented in 32 steps (NS varied from 16 to 192 in dependence of concentration of the sample) from 5 to 95% of its maximum value.
We calculated the diffusion coefficients by analyzing the signal intensity decay as a function of the gradient strength G according to the following equation:

$$ln\frac{I}{I_0} = -(\gamma\delta)^2 D_t(\Delta - \frac{\delta}{3} - \frac{\tau}{2})G^2$$

where I is the observed intensity, I_0 is the non-attenuated signal intensity, D_t is the diffusion translational coefficient, γ is the gyromagnetic ratio of ^1H, and τ is the time between bipolar gradients.

A linear least-squares fitting was used to fit the data

The bound fraction (x) was calculated from the diffusion coefficients [6]

$$X = \frac{D_{Free} - D_{Obs}}{D_{Free} - D_{Bound}}$$

where D_{Free} is the diffusion coefficient of the free ligand, D_{Obs} is the diffusion coefficient observed for the ligand@NC system and D_{Bound} is the expected diffusion coefficient for a ligand bound to a NC surface. The latter was determined using the Stoke-Einstein equation:

$$D = \frac{kT}{6\pi\eta f a}$$

where *k* is the Boltzmann constant, T the temperature in K, η the viscosity of the medium, *f* is the shape factor for cubes (0.66), and *a* the edge length of the NC (10.5 nm).

DDDMAB ligand assignment by using NMR experiments

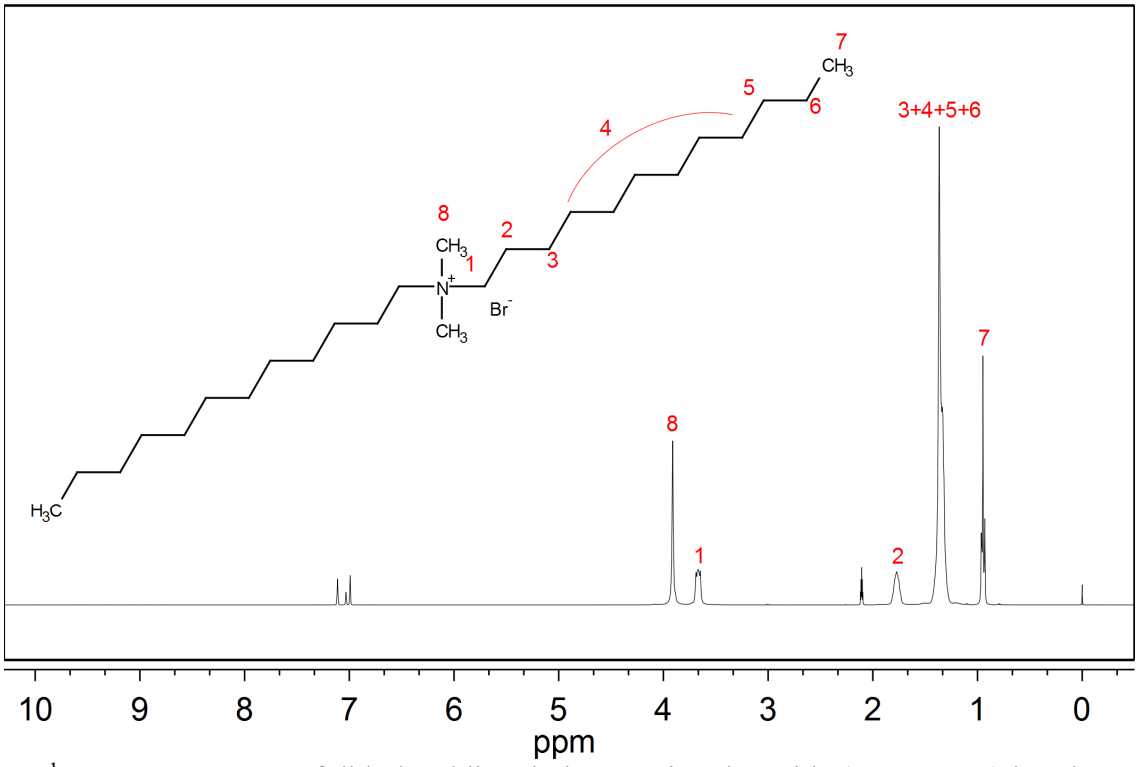

Figure S1: ^{1}H NMR spectrum of didodecyldimethylammonium bromide (DDDMAB) in toluene-d_8 with assignment of signals.

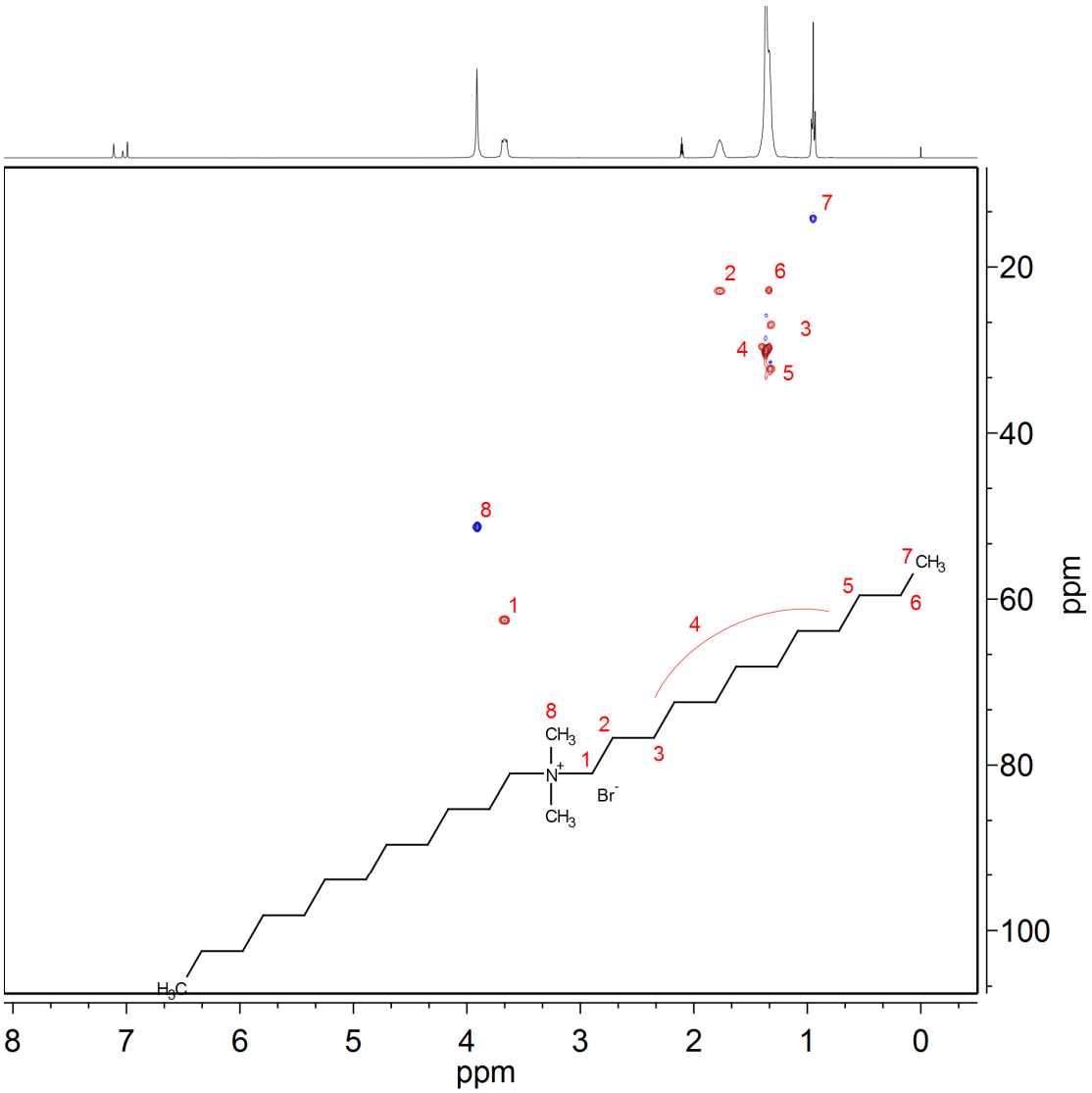

Figure S2: ^{1}H-^{13}C HSQC spectrum of didodecyldimethylammonium bromide (DDDMAB) in toluene-d_8 with assignment of signals.

DDDMAB capped $CsPbBr_3$ NCs, assignment of signals

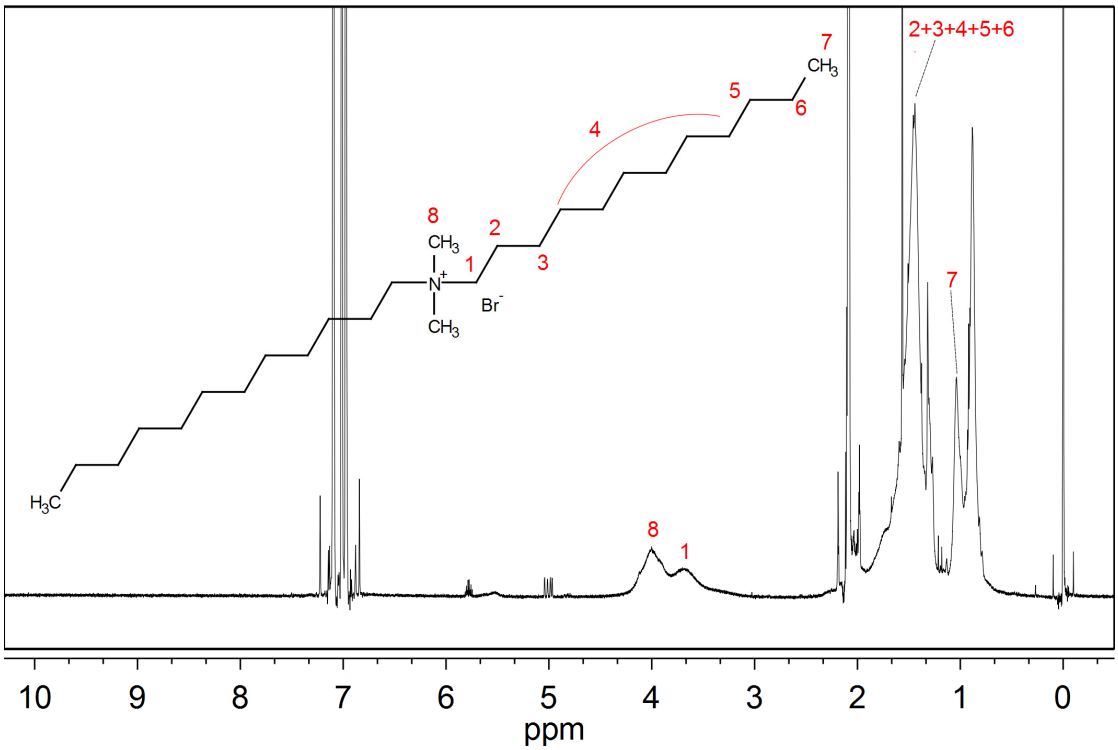

Figure S3: ^{1}H NMR spectrum of DDDMAB capped $CsPbBr_3$ NCs dispersed in toluene-d_8

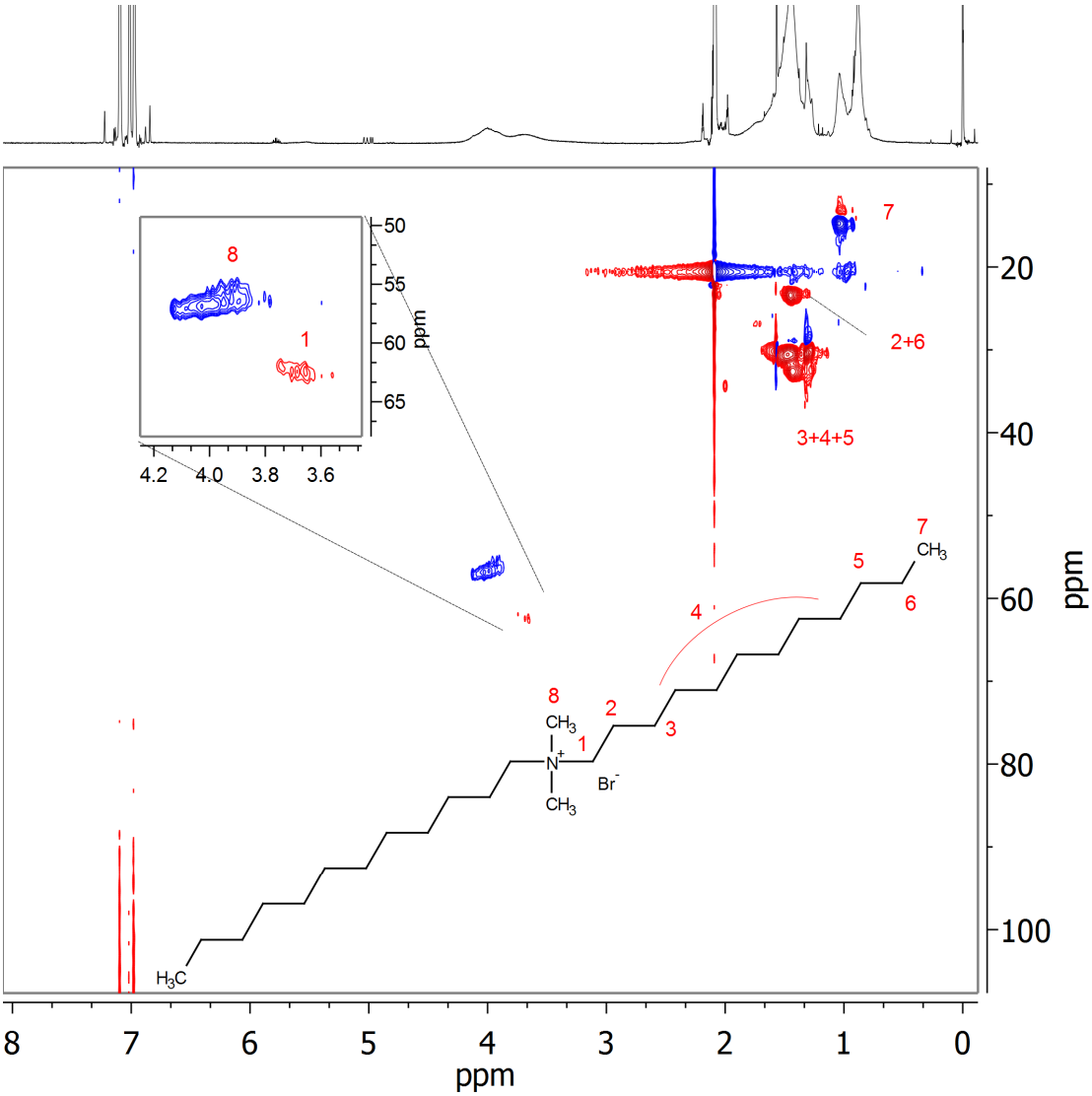

Figure S4: ^{1}H-^{13}C HSQC spectrum DDDDMAB capped $CsPbBr_3$ NCs dispersed in toluene-d_8, with signal assignment

Determining the ligand composition by using *quantitative* NMR

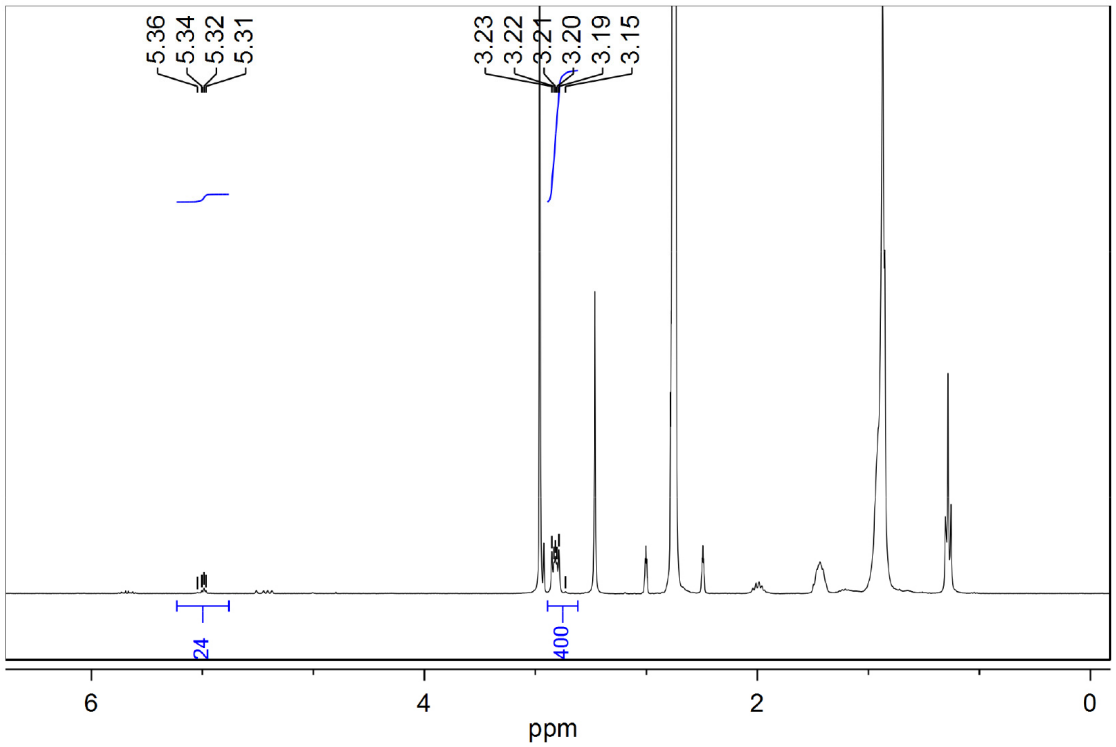

Figure S5: Ligand composition analysis: ^{1}H *q*-NMR spectrum of $CsPbBr_3$ NCs after 1 cycle of ligand exchange with DDDMAB (washed with ethyl acetate) and dissolved in DMSO-d_6 showing 89% replacement of the native Cs-oleate.

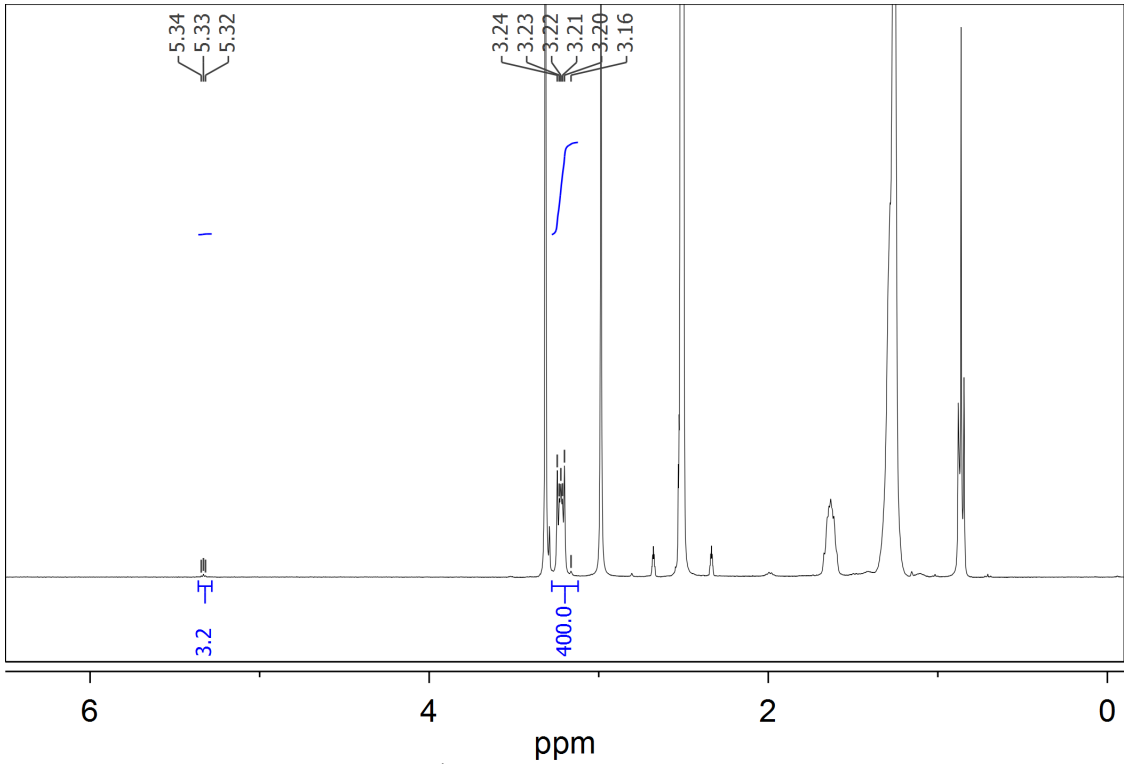

Figure S6: Ligand composition analysis: ^{1}H *q*-NMR spectrum of $CsPbBr_3$ NCs after 3 cycles of ligand exchange with DDDMAB (washed with ethyl acetate) dissolved in DMSO-d_6 evidencing 98% replacement of native Cs-oleate.

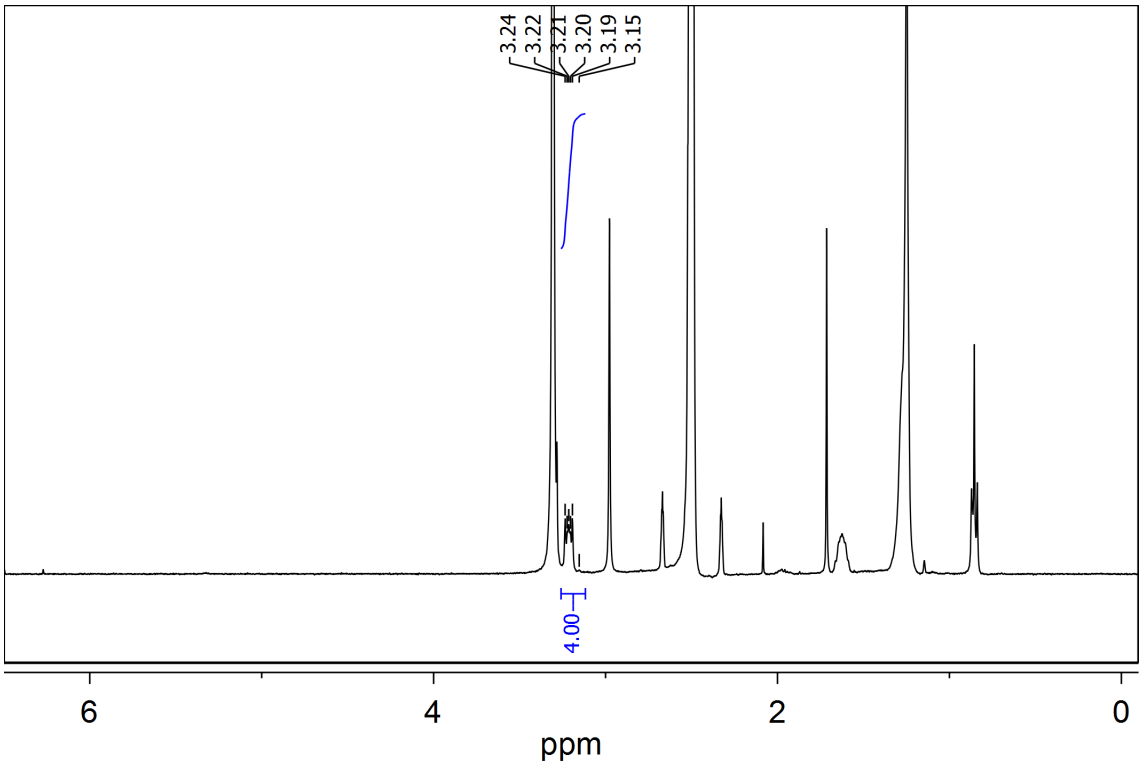

Figure S7: Ligand composition analysis: ^{1}H *q*-NMR spectrum of $CsPbBr_3$ NCs after 3 cycles of ligand exchange with DDDMAB (washed with acetone) and dissolved in DMSO-d_6 evidencing complete ligand exchange.

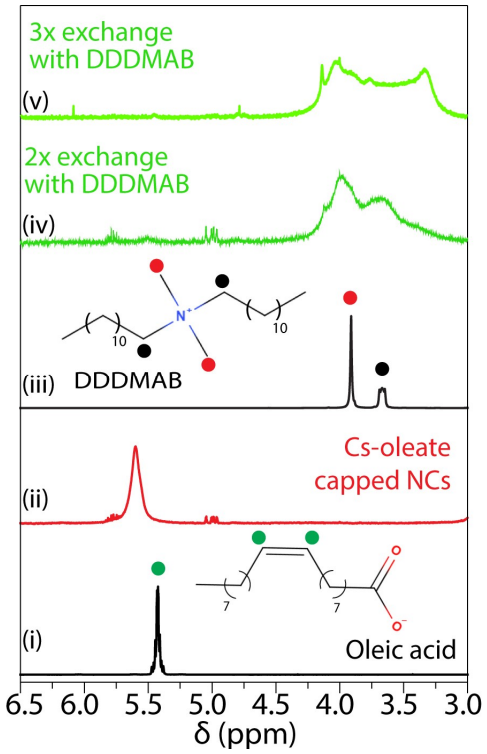

Figure S8: ^{1}H NMR in toluene-d_8 of oleic acid (i), pristine Cs-oleate capped $CsPbBr_3$ NCs (ii), DDDMAB (iii) and $CsPbBr_3$ NCs after two (iv) and three cycles of ligand exchange with DDDMAB (v).

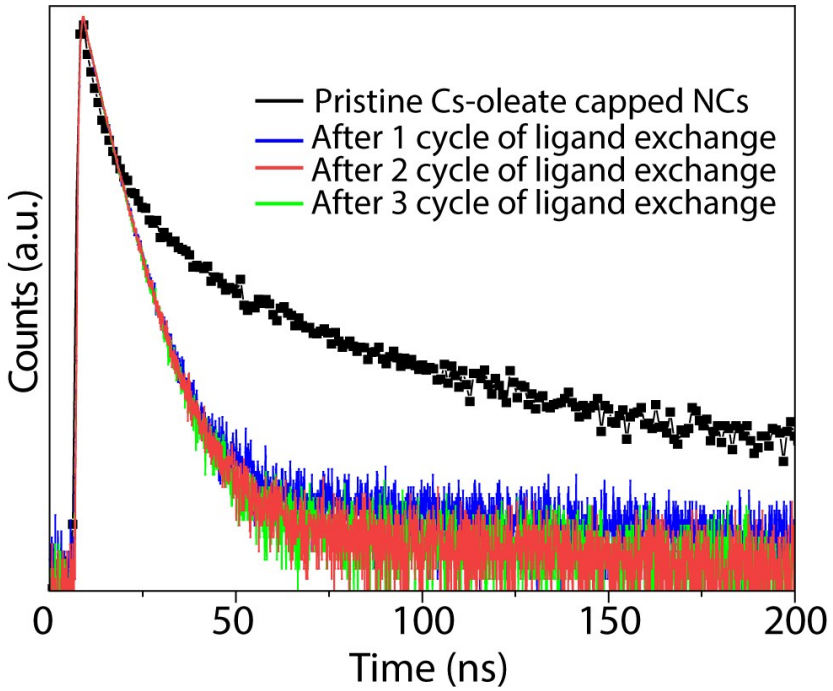

Figure S9: PL decays of dispersions of: pristine (Cs-oleate capped) $CsPbBr_3$ NCs (black dots); NCs after up to 3 cycles of ligand exchange with DDDMAB (blue, red and green traces). NC dispersions exhibit PLQY of 96 ± 5% after 3 cycles of ligands exchange.

Table S1: Photophysical properties of Cs-oleate and Quaternary ammonium capped $CsPbBr_3$ capped NCs

Sample Treated with	eV)	A_1	τ_1 (ns)	A_2	τ_2 (ns)	A_3	τ_3 (ns)	τ_{AVG} (ns)	QY (%)	Γ_{RAD} (1/μs)	$\Gamma_{NON-RAD}$ (1/μs)
Cs-oleate capped NCs	2.41	10062.1	**4.31**	1067.41	**28.05**	129.98	**152.24**	**8.27**	**67**	**80.68**	**40.23**
Didodecyldimethylammonium bromide (DDDMAB)	2.42	10665.3	**5.65**	570.05	**14.59**			**6.11**	99	162.66	1.63
Didecyldimethylammonium bromide (DDMAB)	2.42	8275.16	**5.17**	2047.96	**9.17**	40.99	**37.98**	**6.09**	97	**158.94**	**5.25**
Dioctyldimethylammonium bromide (DODMAB)	2.43	10657	**4.96**	808.59	**13.64**	15.47	**168.42**	**5.79**	95	**164.07**	**8.64**

Morphological evolution of Cs-oleate and DDDMAB capped $CsPbBr_3$ NCs

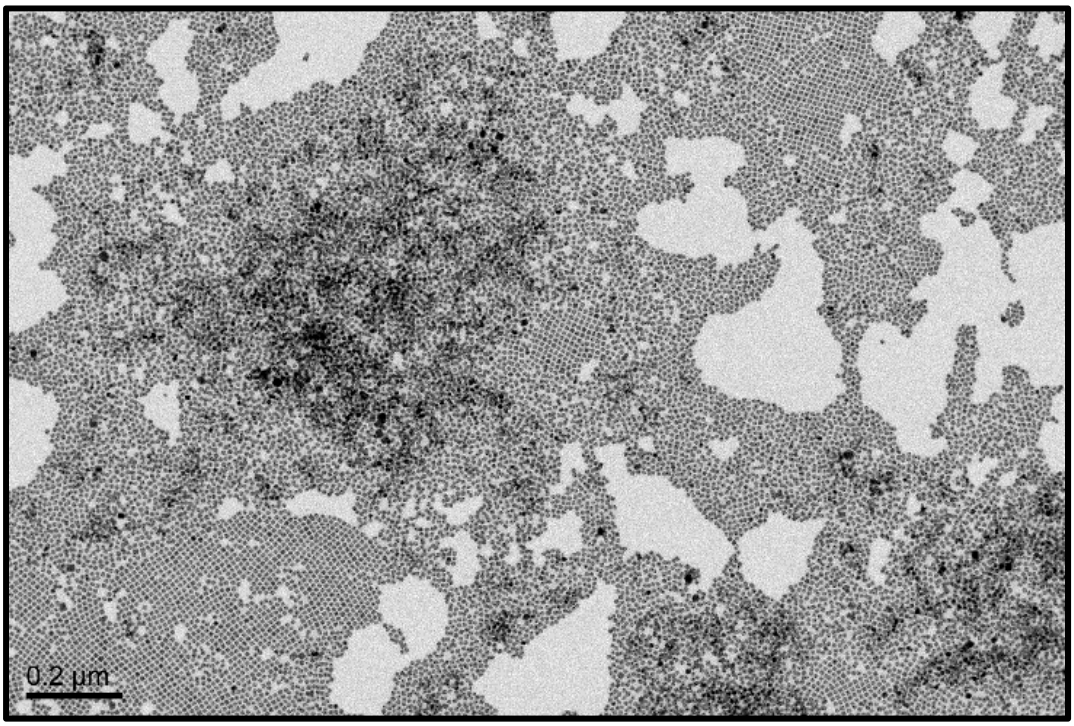

Figure S10: TEM image of Cs-oleate capped $CsPbBr_3$ NCs aged for 3 weeks under air in closed vials.

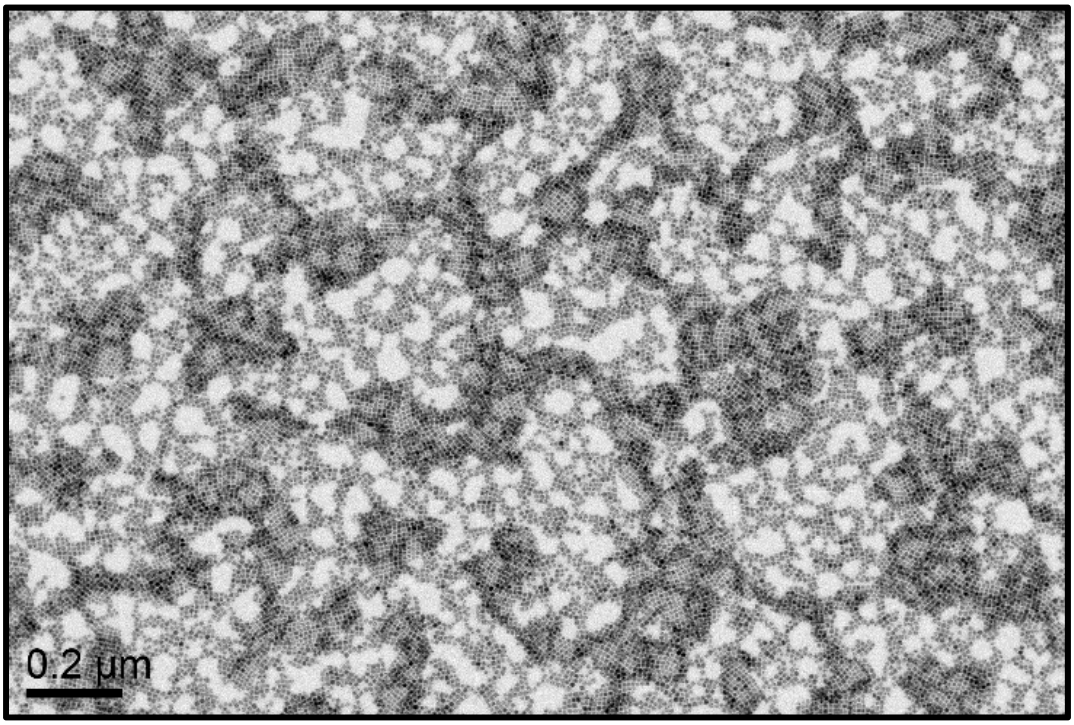

Figure S11: TEM image of DDDMAB capped $CsPbBr_3$ NCs aged for 3 weeks under air in closed vials.

Evolution of structural and optical properties over ageing

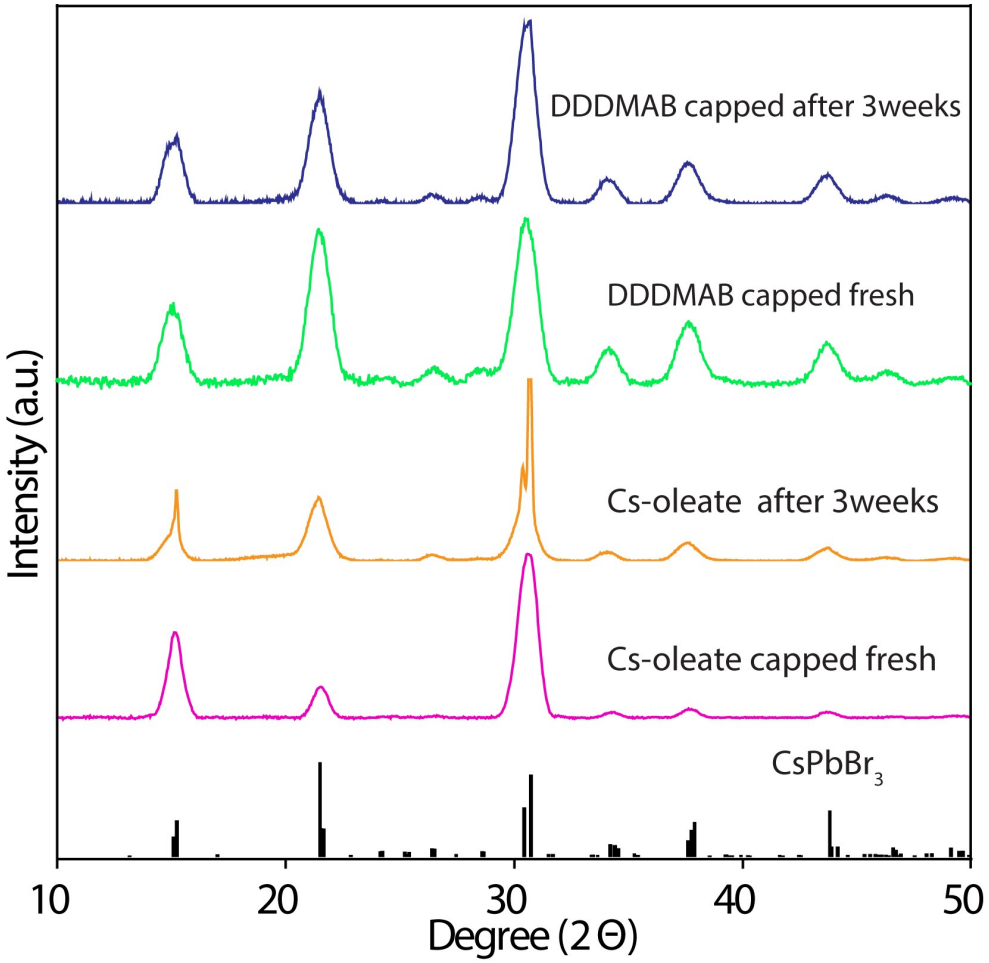

Figure S12: XRD patterns Cs-oleate and DDDAMB capped $CsPbBr_3$ NCs over time with reference (COD 96-451-0746).

Table S2: Photophysical properties of Cs-oleate and Quaternary ammonium capped $CsPbBr_3$ capped NCs fresh and after 3 weeks of storage under ambient conditions

Sample Treated with	eV	A_1	τ_1 (ns)	A_2	τ_2 (ns)	A_3	τ_3 (ns)	τ_{AVG} (ns)	QY (%)	Γ_{RAD} (1/μs)	$\Gamma_{NON-RAD}$ (1/μs)
Cs-oleate capped NCs (fresh)	2.41	10062.1	4.32	1067.41	28.05	129.98	152.24	8.27	67	80.68	40.23
Cs-oleate capped NCs (after 3 weeks)	2.48	4617.28	4.78	4083.88	34.63	1882.72	163.15	44.47	15	3.34	19.14
Didodecyldimethylammonium bromide (DDDMAB) (Fresh)	2.42	10665.3	**5.65**	570.051	**14.59**			**6.11**	99	162.66	1.63
Didodecyldimethylammonium bromide (DDDMAB) (after 3 weeks)	2.42	4739.58	**4.08**	6029.61	**9.57**	72.82	**51.16**	**7.45**	97	129.64	4.59

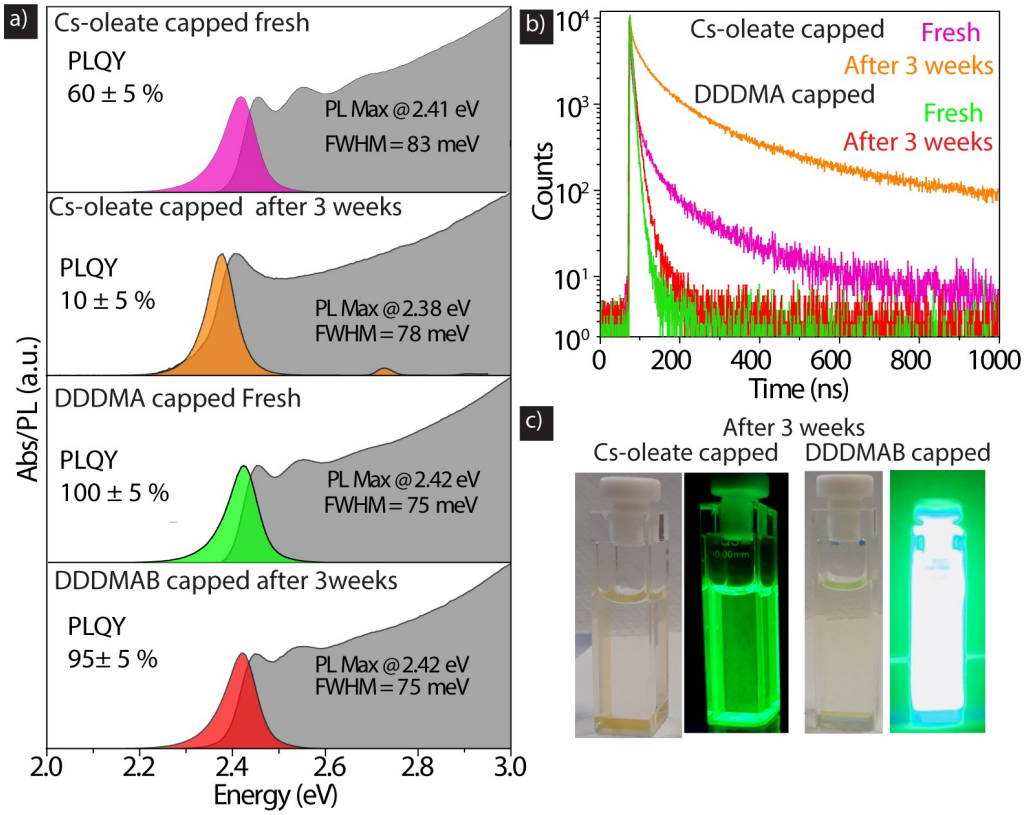

Figure S13: Evolution of the (a) optical absorbance and PL spectra and of the (b) PL decays of Cs-oleate capped and DDDMAB capped $CsPbBr_3$ NC dispersions stored under dilute conditions (at an optical density of 0.1 at 400 nm) over 3 weeks. (c) Photographs (under ambient and UV light) of the dispersions after 3 weeks of storage

DDDMAB treatment on aged Cs-oleate capped $CsPbBr_3$ with low PLQY

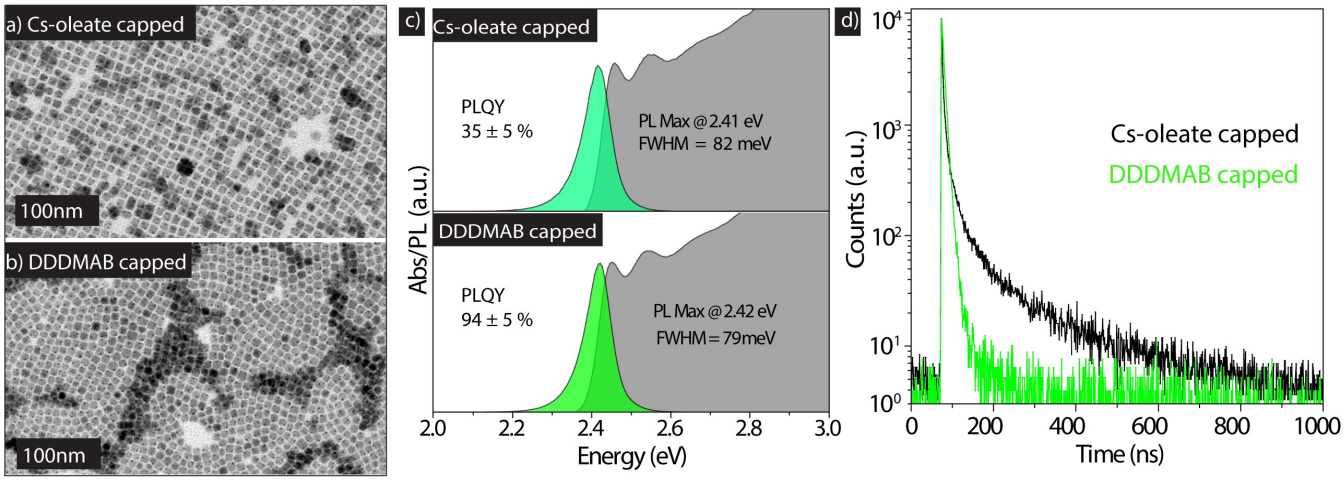

Figure S14: DDDMAB treatment on aged Cs-oleate capped $CsPbBr_3$. TEM images of the (a) aged Cs-oleate capped $CsPbBr_3$ NCs and of the (b) DDDMAB treated NCs, (c) their absorbance and PL spectra and (d) their PL decays.

2D ^{1}H NOESY on DDDMAB capped $CsPbBr_3$ NCs in toluene-d_8 at 300K

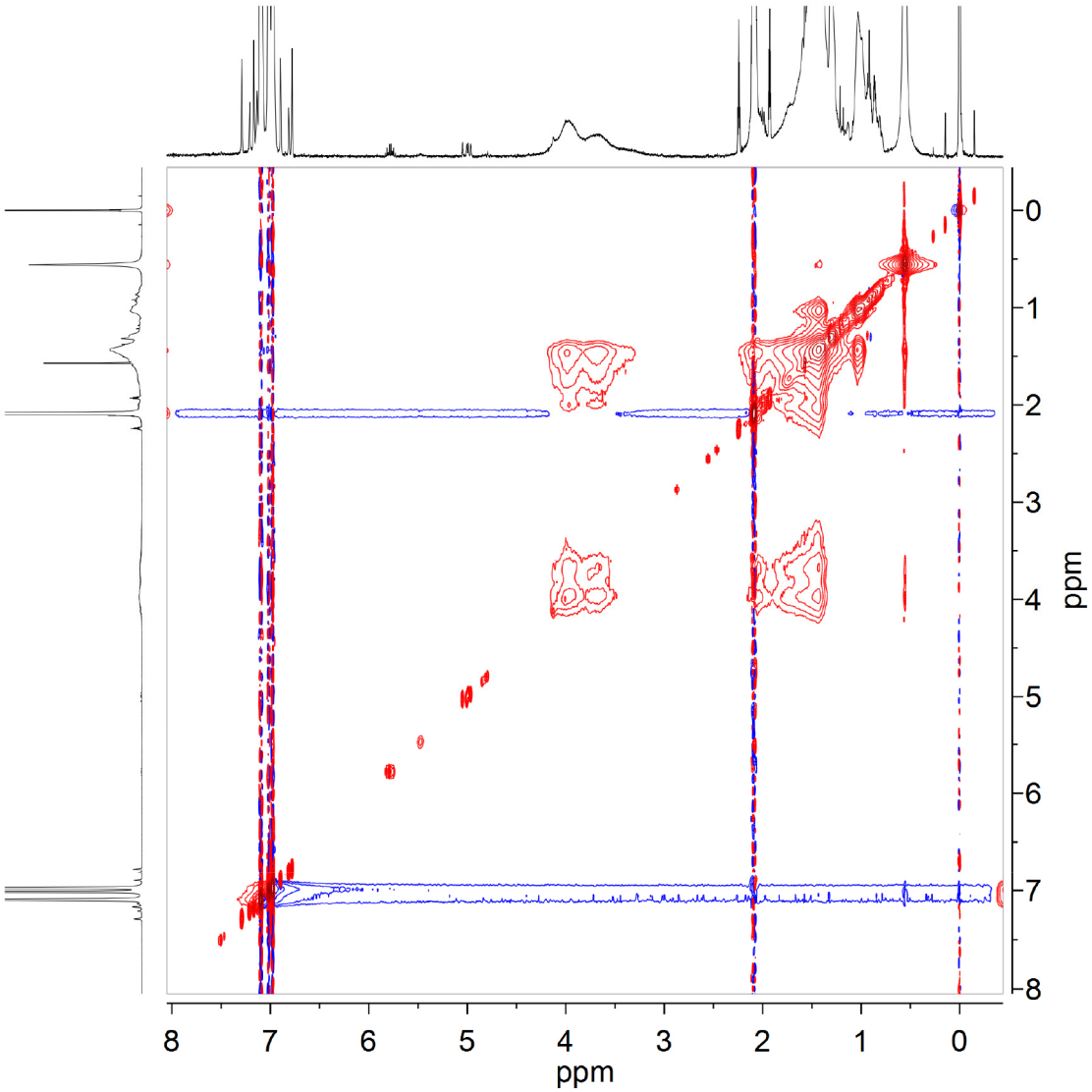

Figure S15: 2D ^{1}H NOESY on DDDMAB capped $CsPbBr_3$ NCs dispersed in toluene-d_8 at 300K

The NOESY experiment returned negative cross peaks (red), typical of species with a reduced mobility in solution (long correlation time, τ_c).

2D ^{1}H NOESY of DDDMAB ligand alone in toluene-d_8 at 300K

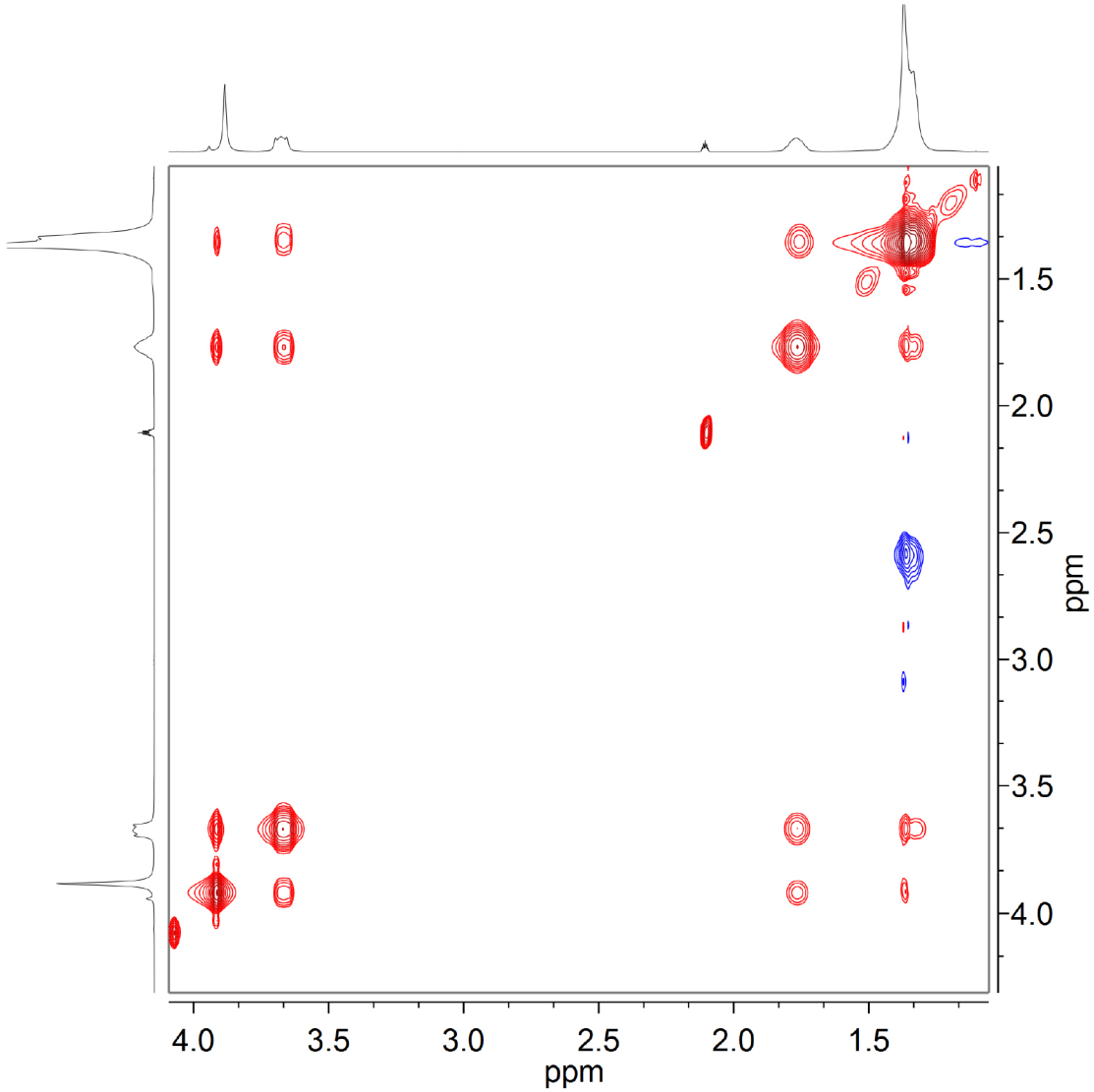

Figure S16: 2D ^{1}H NOESY of a toluene-d_8 solution of DDDMAB at 300K.

Unexpectedly, at 300 K, even the 2D ^{1}H NOESY of DDDMAB ligand alone, showed negative NOE cross peaks (red). We attributed this to the formation of micelles of ligand in solution.

2D ^{1}H NOESY of DDDMAB ligand alone in toluene-d$_8$ at 323K

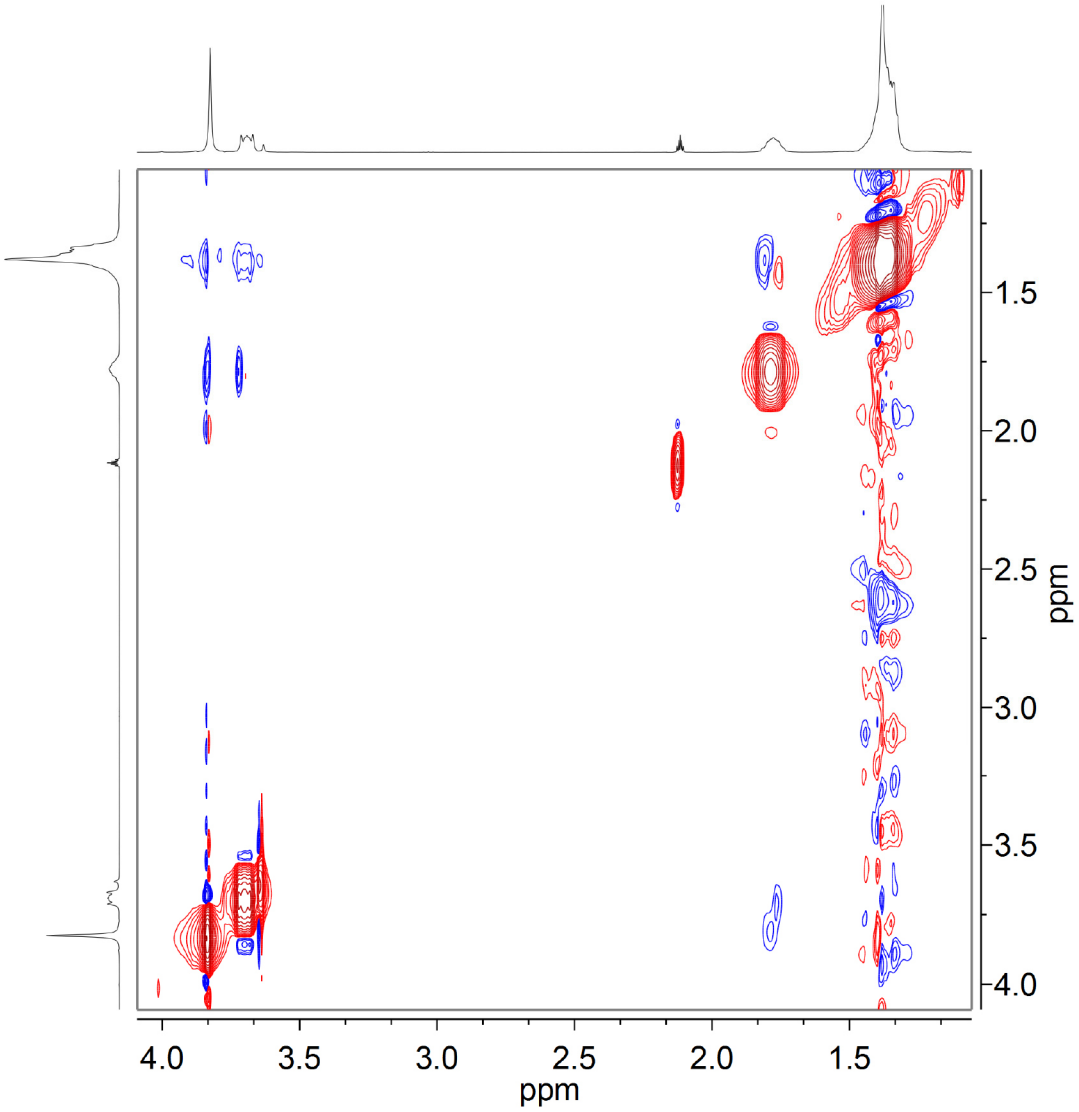

Figure S17: 2D ^{1}H NOESY of a toluene-d$_8$ solution of DDDMAB at 323K.

The 2D ^{1}H NOESY of free ligand at 323 K, shows positive NOE cross peaks (blue), typical of species with small correlation time (τ_c).The Brownian motions at high temperature most likely destroy micelles of ligand.

2D ^{1}H NOESY on DDDMAB capped CsPbBr3 NCs in toluene-d_8 at 323K

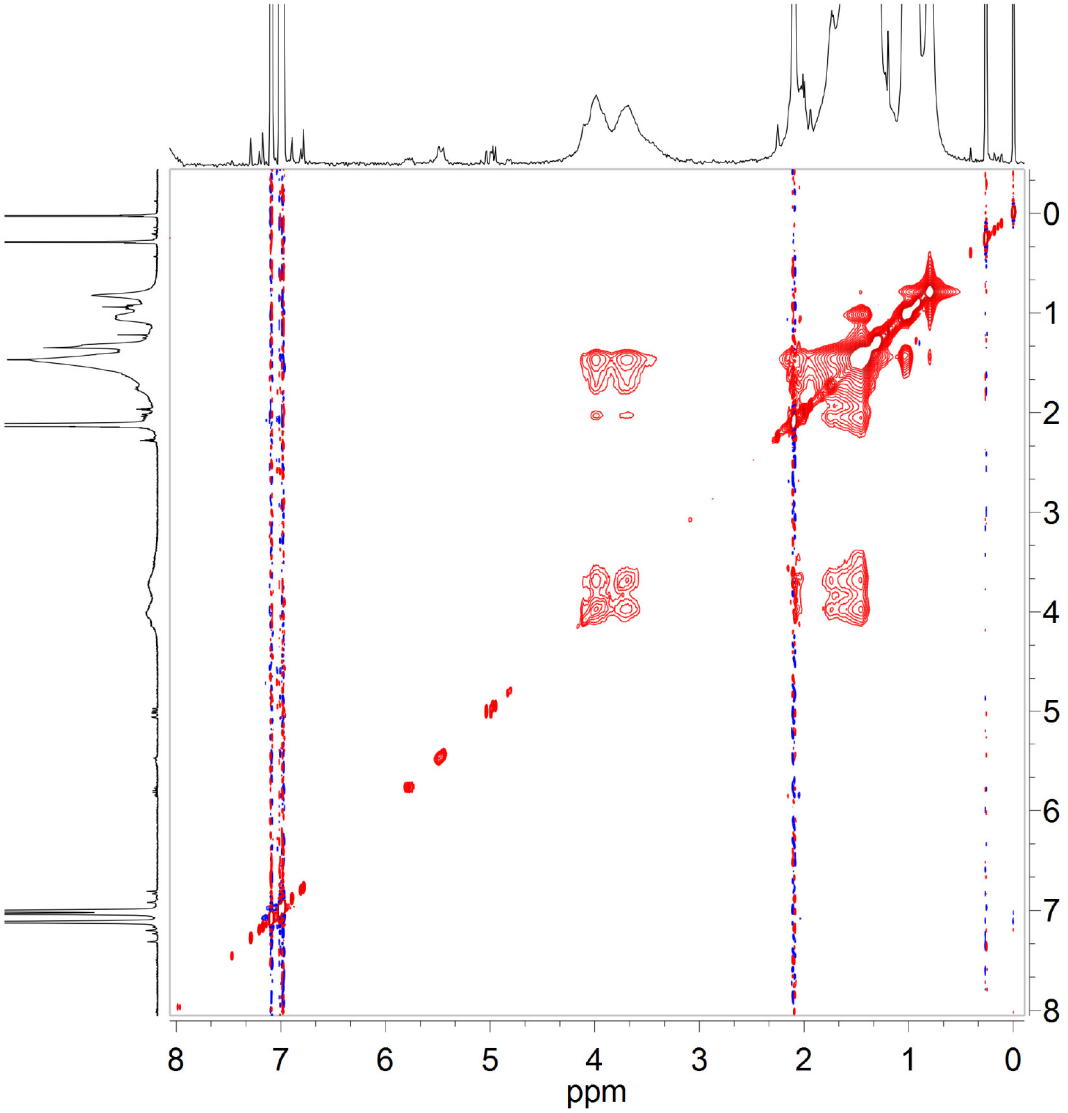

Figure S18: 2D ^{1}H NOESY on DDDMAB capped $CsPbBr_3$ NCs dispersed in toluene-d_8 at 323K.

The negative NOE cross peaks (red) of NC demonstrates that the interaction of ligand with the NCs surface persists even at 323 K.

DOSY on DDDMAB capped $CsPbBr_3$ NCs, in toluene-d_8

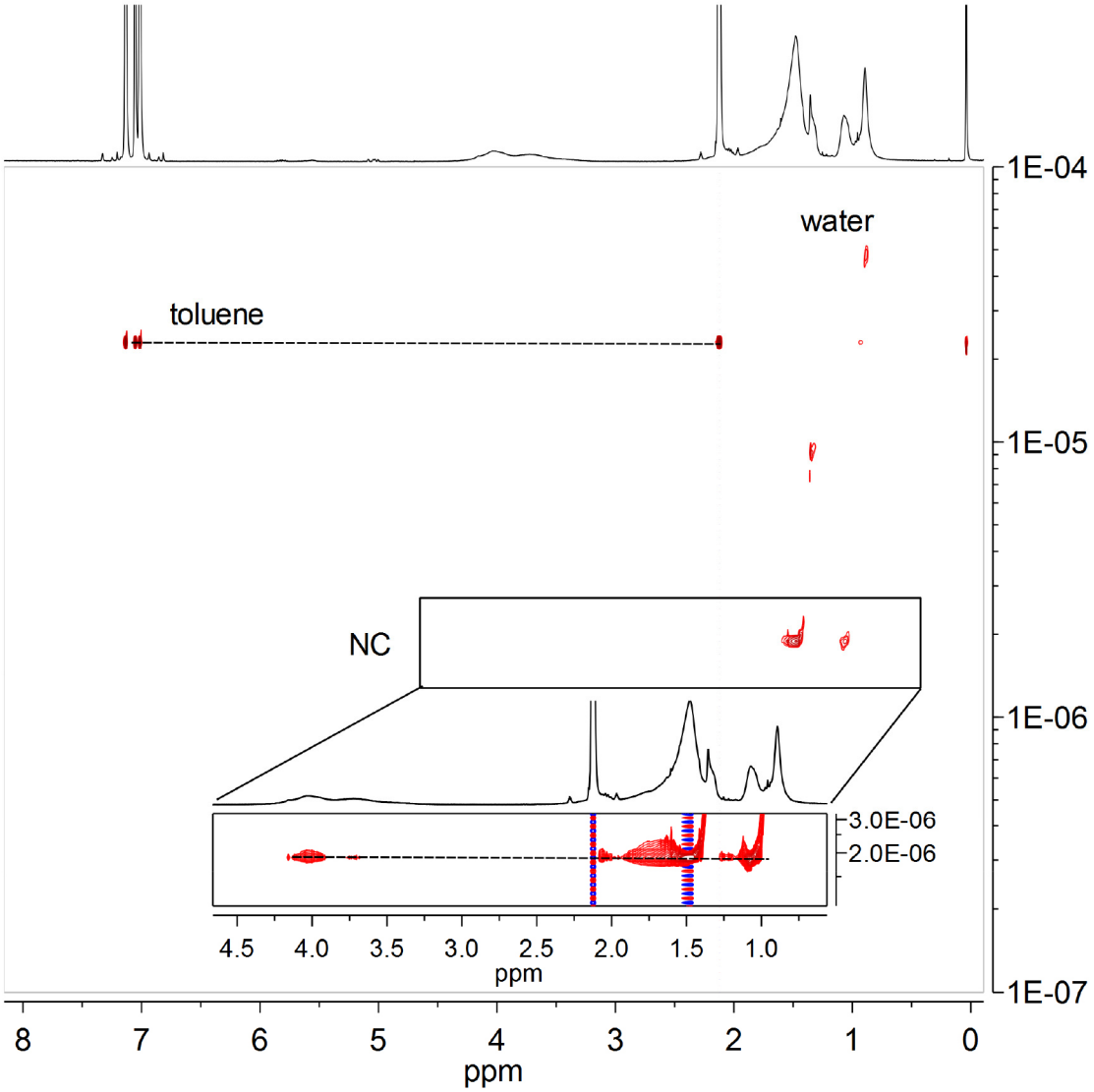

Figure S19: DOSY on DDDMAB capped $CsPbBr_3$ NCs, in toluene-d_8 at 297 K. The inset reports selected rows of the 2D diffusion map showing NC signals only, in order to enhance the CH_3 (8) and CH_2 (1) peak intensity.

DOSY of DDDMAB ligand alone

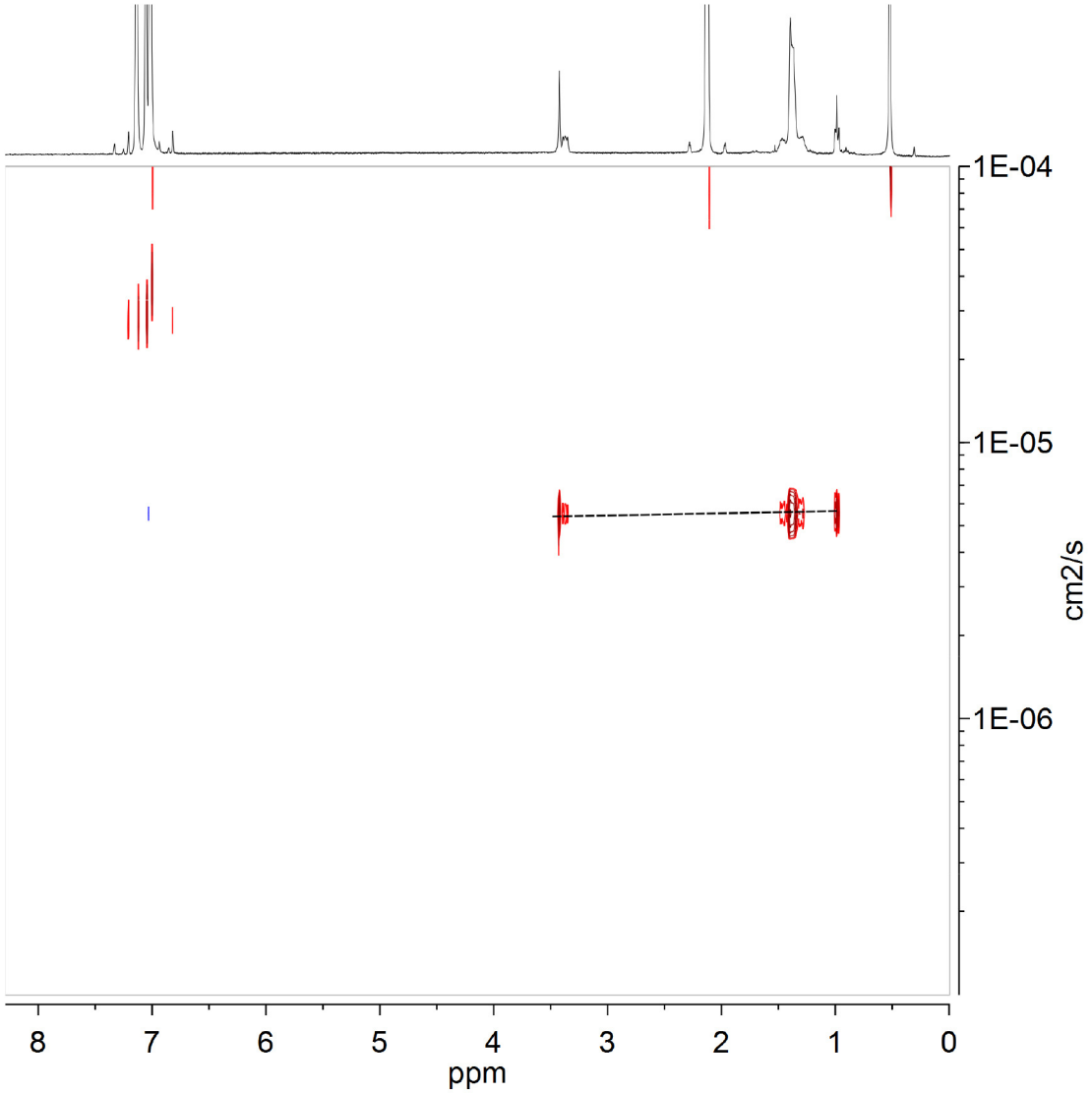

Figure S20: DOSY on DDDMAB free ligand in toluene-d_8 at 297 K**.**

Exploiting the method of De Roo et al.[6] to calculate the bound ligand fraction it is necessary to know the three D values reported in the following equation:

$$x = \frac{D_{free\ ligand} - D_{obs}}{D_{free\ ligand} - D_{bound\ ligand}}$$

The NC@ DDDMAB showed a diffusion coefficient of 170 $\mu m^2/s$ against a theoretical value of ca 48 $\mu m^2/s$ calculated for 8.8 plus 1.6 nm shell for NC@ DDDMAB (size of NCs was calculated from TEM images).

The diffusion coefficient of the DDDMAB ligand alone was found to vary with concentration, most likely due to the formation of reverse-micelles in non-polar solvents. Moreover, the chemical shift of a few resonance i.e. the CH_3 (8) and CH_2 (1 and 2) significantly shifted upon concentration increase (Figure S21), while the other CH_2 and the terminal CH_3 groups of the aliphatic side chain were unaffected. From the shift in the ^1H signal vs. [DDDMAB] (see Figure S21), we inferred a critical micellar concentration (CMC) of 0.35 mM. The diffusion coefficient of DDDMAB at concentrations lower than CMC is 540 $\mu m^2/s$.

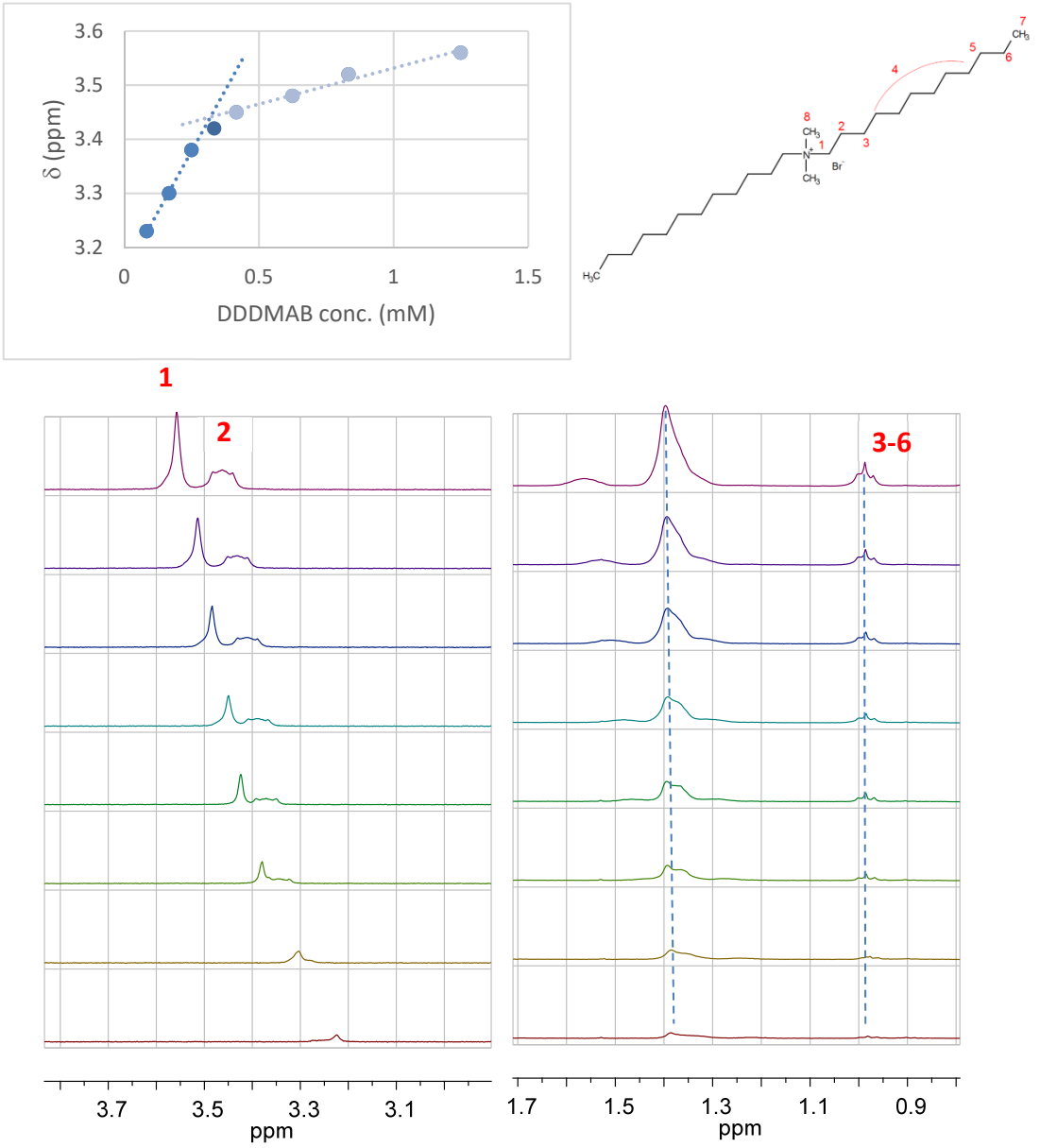

Figure S21. ^1H NMR of DDDMAB solutions in toluene-d_8 of increasing concentration and trend of the chemical shift of CH_3 (8) resonance vs [DDDMAB].

Ligand exchange with shorter (<C_{12}) chain quaternary ammonium bromides

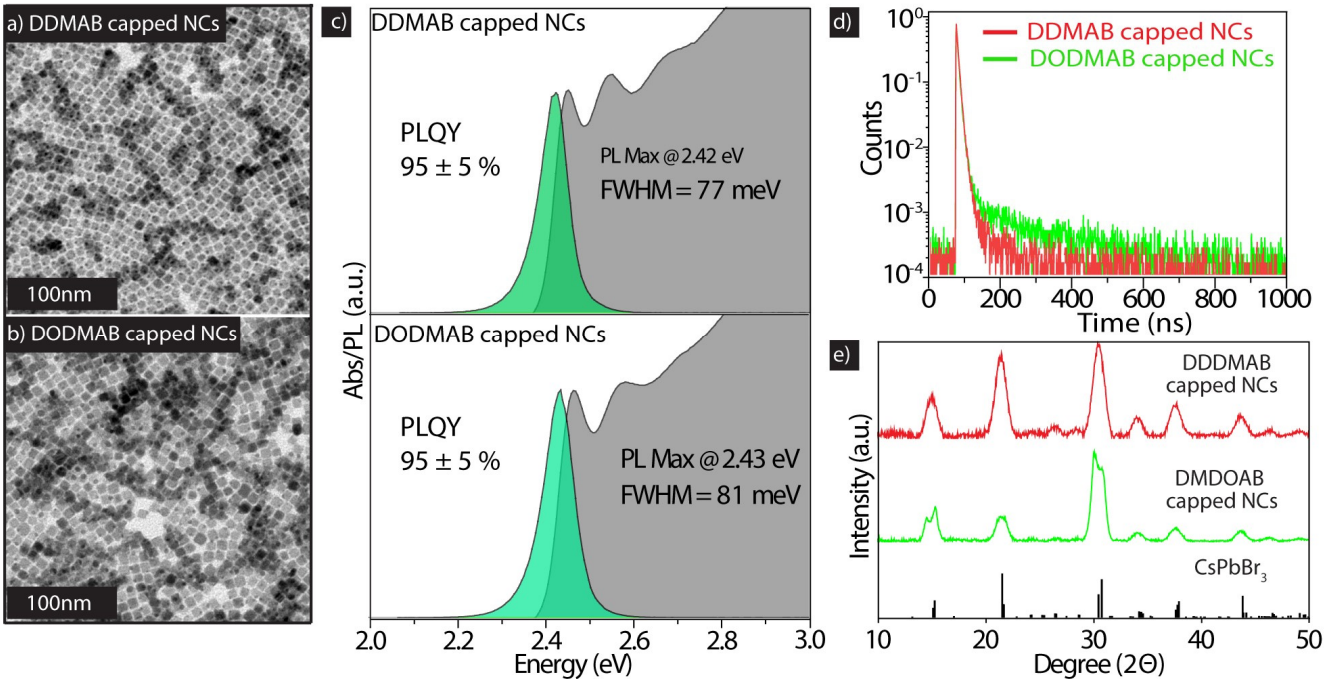

Figure S22: TEM images of $CsPbBr_3$ NCs after treatment with (a) DDMAB (didecyldimethylammonium bromide) and (b) DODMAB (dioctyldimethylammonium bromide). (c) Absorbance, PL spectra, and their (d) PL lifetimes. (e) XRD reference patterns of corresponding samples with reference (COD 96-451-0746).

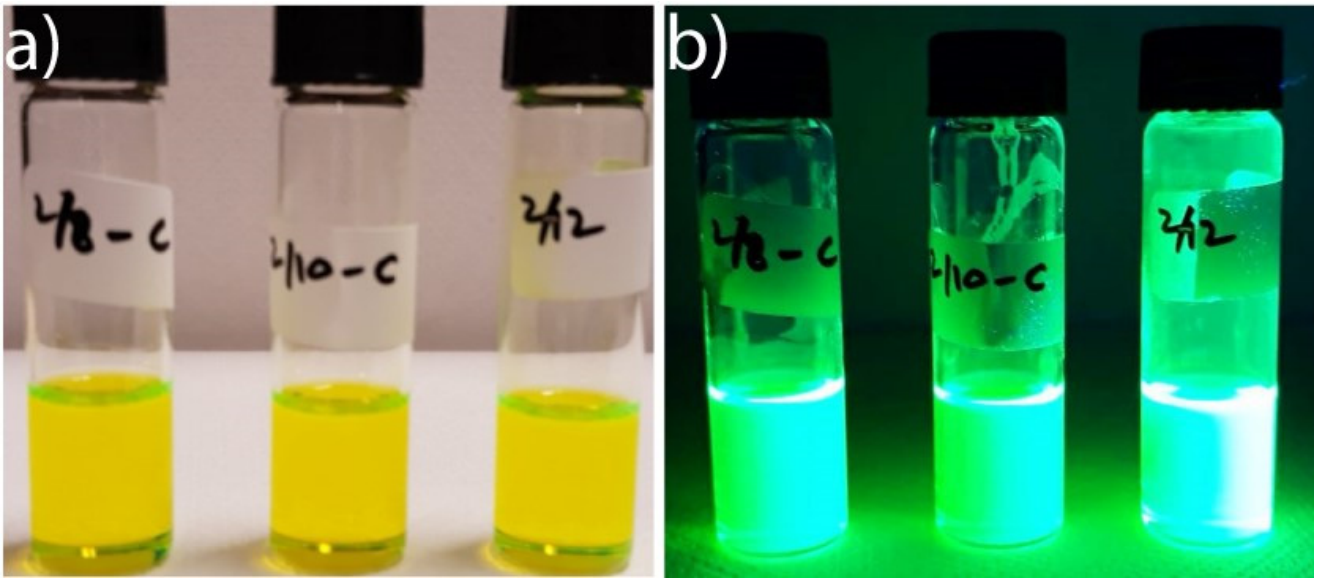

Figure S23: Left to right, Photos of $CsPbBr_3$ nanocubes after ligand exchange with DODMAB (dioctyldimethylammonium bromide), DDMAB (didecyldimethylammonium bromide) and DDDMAB (didodecyldimethylammonium bromide) under (a) ambient light and (b) UV lamp.

DFT Calculations

In Figure S24 we show a comparison of the anchoring of a secondary and a quaternary ammonium bromide with a short methyl chain on the CsBr terminated NC where one of the Cs was replaced with the ammonium species. The secondary amine anchors on the NC with two C atoms and the N atom in the same plane, parallel to the NC surface (red circle). This limits the penetration of the anchoring group into the Cs site. Meanwhile, the quaternary amine arranges so that only the CH_3-N bond is orthogonal to the surface, releasing the strain between alkyl chains that facilitates a higher passivation of the NC.

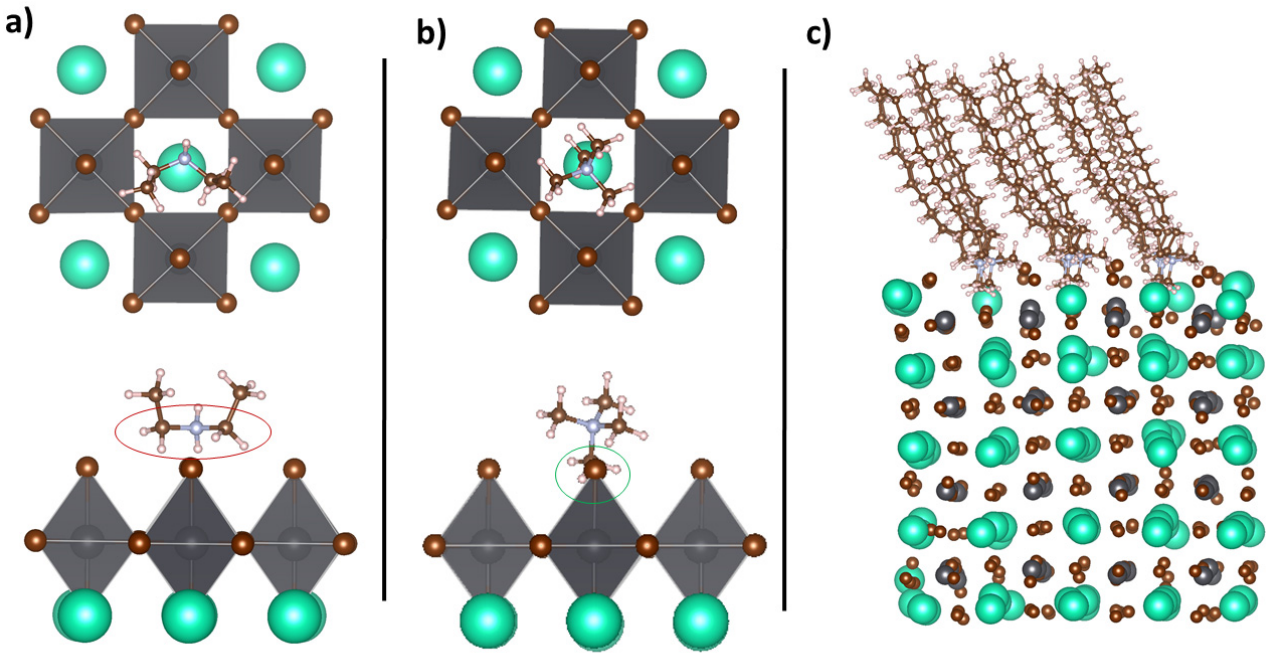

Figure S24: Schematic representation of the binding of (a) secondary and (b) quaternary ammonium bromides (dimethylammonium and tetramethylammonium bromides) onto a $CsPbBr_3$ surface after relaxation of the structure at the DFT/PBE level of theory. Cs atoms are represented with green spheres, Pb atoms are shown in grey, Br and C in brown and H in white. (c) 2.4 nm (edge length) $CsPbBr_3$ NC with 9 DDDMAB ligands passivating one facet: this configuration was used to calculate the steric repulsion between ligands.

Additional ligand exchange reactions

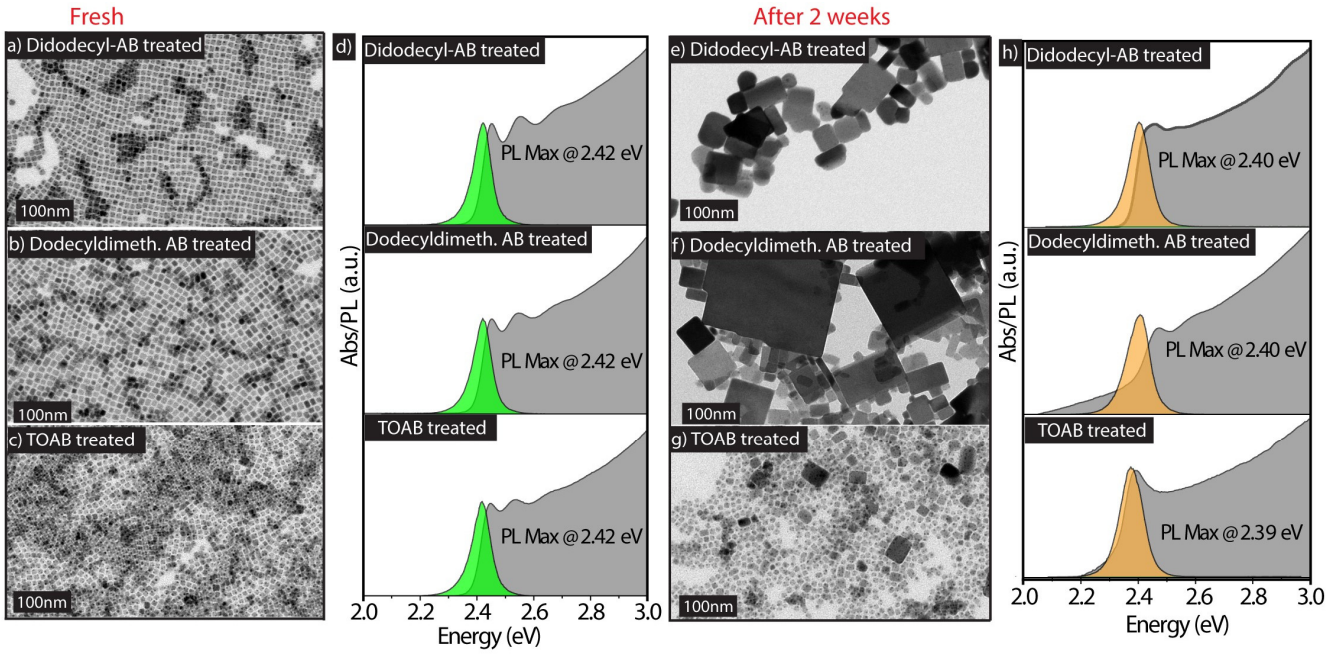

Figure S25: TEM images of $CsPbBr_3$ NCs fresh exchanged (left panels), and two weeks after the exchange (right panels) with: Didodecylammonium bromide (a, e) dodecyl dimethylammonium bromide (b, f) and tetraoctylammonium bromide (TOAB) (c, g), along with their optical features (d, h).

References

1. Imran, M.; Ijaz, P.; Baranov, D.; Goldoni, L.; Petralanda, U.; Akkerman, Q.; Abdelhady, A. L.; Prato, M.; Bianchini, P.; Infante, I.; Manna, L., *Nano Lett.* **2018** *18*, 7822-7831.
2. Hutter, J.; Iannuzzi, M.; Schiffmann, F.; VandeVondele, J., *Wiley Interdiscip. Rev. Comput. Mol. Sci.* **2014,** *4*, 15.
3. Perdew, J. P.; Burke, K.; Ernzerhof, M., *Phys. Rev. lett.* **1996,** *77*, 3865.
4. VandeVondele, J.; Hutter, J., *J. Chem. Phys.* **2007,** *127*, 114105.
5. (a) ten Brinck, S.; Infante, I., *ACS Energy Lett.* **2016,** *1*, 1266. (b) Krieg, F.; Ochsenbein, S. T.; Yakunin, S.; Ten Brinck, S.; Aellen, P.; Suess, A.; Clerc, B.; Guggisberg, D.; Nazarenko, O.; Shynkarenko, Y.; Kumar, S.; Shih, C. J.; Infante, I.; Kovalenko, M. V., *ACS Energy Lett.* **2018,** *3*, 641.
6. De Roo, J.; Ibanez, M.; Geiregat, P.; Nedelcu, G.; Walravens, W.; Maes, J.; Martins, J. C.; Van Driessche, I.; Kovalenko, M. V.; Hens, Z., *ACS Nano* **2016,** *10*, 2071.